Imaging dispersion curves of passive surface waves

Choon Park, Richard Miller, David Laflen, Cabrilo Neb, Julian Ivanov, and Brett Bennett, Kansas Geological Survey, and Rob Huggins, Geometrics, Inc.*

Summary

A scheme to process passive surface waves is briefly described. It transforms wavefields of horizontal plane-wave propgation, measured with receiver spreads along the two orthogonal axes (*x* and *y*), into dispersion images. The scheme first transforms the measured wavefields of a particular frequency (ω) into the energy in phase velocity (*c*)-azimuth (θ) space where multiple sources and modes of surface waves are represented as energy peaks at different azimuths and phase velocities, respectively. The scheme, then, stacks all the energy through the azimuth axis to produce an energy distribution along the phase-velocity (*c*) axis only. A final image is then created by repeating these steps for different frequencies and displaying the energy in frequency (ω)-phase velocity (*c*) space. This process greatly alleviates general complications with the passive method such as disturbance of phase velocities due to multiple sources and modes as well as the spatial aliasing.

Introduction

As the surface-wave method is gaining in popularity among engineers and geophysicists, demand for increased investigation depth is also growing. However, the amount of active-source energy to gain a few more hertz at the low-frequency end of a dispersion curve often increases by several orders of magnitude, rendering efforts with an active source impractical and uneconomical. On the other hand, passive surface waves generated from natural (e.g., tidal motion) or cultural (e.g., traffic) sources are usually of a low-frequency nature with wavelengths ranging from a few kilometers (natural sources) to a few tens (or hundreds) of meters (cultural) (Okada, 2003), providing a wide range of penetration depths and therefore a strong motivation to utilize them.

In the passive case, however, complications arise because of the unknown characteristics such as location (azimuth and distance), strength, and number of sources, and also single- or multi-modal nature of surface waves. The conventional 1-D receiver array survey method is therefore incapable of adequately resolving all these issues. Instead, a cross-layout receiver spread deployed along two orthogonal (*x* and *y*) axes can be a better alternative (Figure 1). The data processing scheme is briefly described here and a more extensive coverage will be found in Park et al. (2004). The scheme images dispersion trends of all existing modes of horizontal plane-wave propagation and has been developed by extending the scheme by Park et al. (1998) normally used in the active surface-wave method (MASW) (Park et al., 1999) using an 1-D receiver spread.

Passive surface wave utilization has been intensively studied in Japan under the microtremor survey method (MSM) (Okada, 2003) developed to utilize surface waves recorded at earthquake stations. Both beam-forming (*f-k*) and spatial autocorrelation (SPAC) methods are used to process MSM data. An excellent review of the MSM can be found in Okada (2003). Using the frequency-wavenumber (*f-k*) method, Asten and Henstridge (1984) processed microseisms recorded with seven seismometers deployed along a cross-layout configuration in a nonlinear fashion over several kilometers of distance. Recently, several research groups attempted to apply the MSM to the near-surface investigation (down to10's-100's meters) by using conventional exploration seismic instruments (Haruhiko and Hayashi, 2003; Yoon and Rix, 2004). Louie (2001) developed a scheme to process passive surface waves recorded with a 1-D receiver array commonly used for a conventional body-wave (e.g., refraction) survey.

Data Processing Scheme for 2-D Cross Layout

A scheme to process the passive data acquired by using a 2-D cross layout (Figure 1) has been developed by extending the scheme by Park et al. (1998) normally used in the active 1-D MASW surveys. This 1-D scheme is similar to applying the slant-stack (τ-*p*) process in the frequency domain, and is often considered as a composite scheme of the slant-stack and the conventional frequency-wavenumber (*f-k*) methods. It usually achieves a higher resolution in imaging the dispersion trend and is more straightforward in calculation scheme than are the other two methods (Park et al., 1998; Moro et al., 2003). With the 1-D scheme, to calculate the relative energy, $E_{1\text{-D}}(\omega,c)$, for a particular frequency (ω) and a scanning phase velocity (*c*), it first applies the necessary phase shift ($\phi_i=\omega x_i/c$) to the Fourier transformation, $R_i(\omega)$, of the *i-th* trace, $r_i(t)$, at offset x_i, sums all (*N*) phase-shifted traces, and then takes absolute value of the summed complex number:

$$E_{1-\text{D}}(\omega,c)=\left|\sum_{i=1}^{N} e^{j\phi_i} R_i(\omega)\right| \qquad (1)$$

This scheme for a 1-D survey, therefore, has two scanning parameters; frequency (ω) and phase velocity (*c*). The dispersion image is created by scanning through a preset range of frequency and phase velocity.

In the case of a 2-D passive survey, another parameter is added for scanning: the azimuth (θ) of incoming surface waves. For each frequency (ω), the energy, $E_{2\text{-D}}(\omega,c,\theta)$, for a scanning phase velocity (*c*) is calculated by assuming an azimuth (θ). This calculation is carried over scanning range of the phase velocity (for example, 50 m/sec-3000 m/sec with 10

m/sec increment), and then over that of the azimuth (for example, 0-360 degrees in 5-degree increments) (Park et al., 2004):

$$E_{2-\mathrm{D}}(\omega,c,\theta)=\left|\sum_{ix=1}^{NX}e^{j\phi_{ix}}R_{ix}(\omega)+\sum_{iy=1}^{NY}e^{j\phi_{iy}}R_{iy}(\omega)\right| \qquad (2)$$

Because of two orthogonal receiver spreads, the summation is carried over *NX* and *NY* traces along *x* and *y* axes, respectively. For given *c* and θ, the necessary phase shift ϕ_{ix}=-$\omega x_{ix}\cos\theta/c$ (or ϕ_{iy}=-$\omega y_{iy}\sin\theta/c$) for a trace at $x=x_{ix}$ (or $y=y_{iy}$) is calculated based on the projection principle (Figure 1) that incorporates *c* and θ into a vector. Since there is no one fixed source point in the 2-D passive case, however, there can be no absolute origin (for example, *x*=0 for 1-D active case). However, the equation (2) does not need such an origin (Park et al., 2004). Instead, any relative coordinate system that conforms to actual field scale will yield equally the same results. For a descriptive convenience, an arbitrary origin (*x*=0 and *y*=0) is set at the crossing point of *x* and *y* receiver spreads (Figure 1).

In the space of *c* and θ for a given ω, there can be multiple energy peaks occurring at different phase velocities and azimuths, representing different modes and sources, respectively. Also, different amplitudes of these peaks can represent different energy partitioning between modes or different strengths of the source or both. To fully account for all these possibilities, all the energy in *c*-θ space is stacked along the azimuth (θ) axis for N_θ different azimuths to produce $E'_{2\text{-D}}(\omega,c)$:

$$E'_{2-\mathrm{D}}(\omega,c)=\sum_{i=1}^{N_\theta}E_{2-D}(\omega,c,\theta_i) \qquad (3)$$

Those energy peaks of the same mode but from different sources are constructively stacked. This stacking allows a full exploitation of multi-modal and multi-source nature of passive surface waves.

Fundamental concepts of the aforementioned passive scheme are further illustrated through modeling. A 48-channel cross layout with a 5-m receiver spacing was modeled with ten (10) sources whose locations and strengths were arbitrary chosen (Figure 2a). Dispersion curves used are displayed in Figure 2b for the two modes (M0 and M1). The strength of the second mode (M1) was assumed to be half that of the first mode (M0). The modeling scheme tries to closely mimic not only the dispersion but also the attenuation of surface waves (Park et al., 2004). Two different output records were generated from the modeling; one (Figure 2c) with a single mode (M0) and the other (not shown) with both modes (M0 and M1). Values of $E_{2\text{-D}}(\omega,c,\theta)$, equation (2), calculated for an arbitrary frequency of 23 Hz are plotted in Figures 3a and 4a for the two modeled cases. Values of $E'_{2\text{-D}}(\omega,c)$, equation (3), stacked over all azimuths are also plotted on the right side of each display. Final dispersion images are then created by performing the calculation of $E'_{2\text{-D}}(\omega,c)$ over all the scanning frequencies and displayed in Figures 3b and 4b for the scanning range of 5 Hz-50 Hz with 0.1-Hz increment.

Field Data with Cross Layout

Sets of 48-channel passive surface wave data were acquired at a soccer field of the Kansas University (KU), Lawrence, Kansas (Figure 5a). The field record displayed in Figure 5b was obtained by vertically stacking ten (10) such records individually acquired with 20-sec recording time. Nearby streets had fairly heavy traffic during the survey with occasional passage of heavy trucks. Receivers were 4.5-Hz geophones laid with 5-m spacing along the *x* and *y* axes.

The dispersion image displayed in Figure 5c was constructed by using the scheme previously outlined. Two modes (M0 and M1) are clearly identified and interpreted to be the fundamental and a higher modes, respectively. The non-dispersive trend visible above 20 Hz as a straight horizontal streak has a constant phase velocity of 350 m/sec and is interpreted as air waves (at 25°C). To assess effectiveness of the passive method, several active records were also acquired by using a 1-D receiver array (with 5-m spacing) and 20-lb sledge hammer as the seismic source. Several different source offsets were tested in an attempt to maximize the recording of low-frequency energy as much as possible. The dispersion image in Figure 5d was obtained from one of those active records that met this purpose best. The fundamental-mode dispersion curve was extracted in the 8-50 Hz range (Figure 5c). The lower-frequency portion (8-20 Hz) was extracted from the passive image (Figure 5c), whereas the rest (20-50 Hz) was more confidently extracted from the active image (Figure 5d). Vertical Vs variation at the surveyed site was obtained for an approximate depth range of 0-80 m (Figure 5e) by inverting the extracted dispersion curve using the algorithm by Xia et al. (1999).

Discussions and Conclusions

When multiple sources are involved, energy peaks in *c*-θ space (Figures 3a and 4a) may not always occur at the correct values of *c* and θ. Instead, they tend to be disturbed around correct values randomly. This disturbance seems to be aggravated as the numbers of source and mode contributing to the measurement increase. In addition, there can be peaks generated from spatial aliasing. These phenomena are common to all the existing processing methods (Okada, 2003). However, stacking along the azimuth axis significantly cancels out this disturbance as well as the spatially-aliased peaks (although not complete as can be seen from the unsmooth dispersion images).

One of the underlying assumptions for the presented scheme as well as the beam-forming method is the plane-wave propagation of surface waves. The degree of violation depends

on the vicinity of sources that in turn depends on wavelength and receiver spread length (L) along one of the axes. As a rule of thumb, L needs to be about the same as (or greater than) the maximum investigation depth and the passive sources need to be located outside the circumference defined by the two axes. Considering the near-field effects possibly involved, however, this source distance may need to be more conservative (for example, twice the radius of the circumference). Detailed discussion of all these issues as well as the issue of field layout will be found in Park et al. (2004).

It is concluded at this stage of the study that imaging the dispersion trends of the passive surface waves can be accomplished by extending the imaging scheme (Park et al., 1998) used to process active surface waves. Advantages of the presented scheme are those capabilities of 1) imaging (instead of calculating) dispersion trends, 2) minimizing the disturbance and the spatial-aliasing effects and therefore maximizing the analysis accuracy, and 3) simplicity in algorithm.

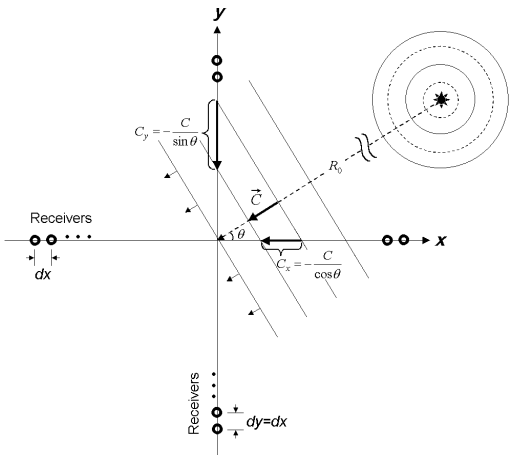

Figure 1. Schematic of a cross-layout receiver spread used for the multi-channel analysis of passive surface waves method outlined.

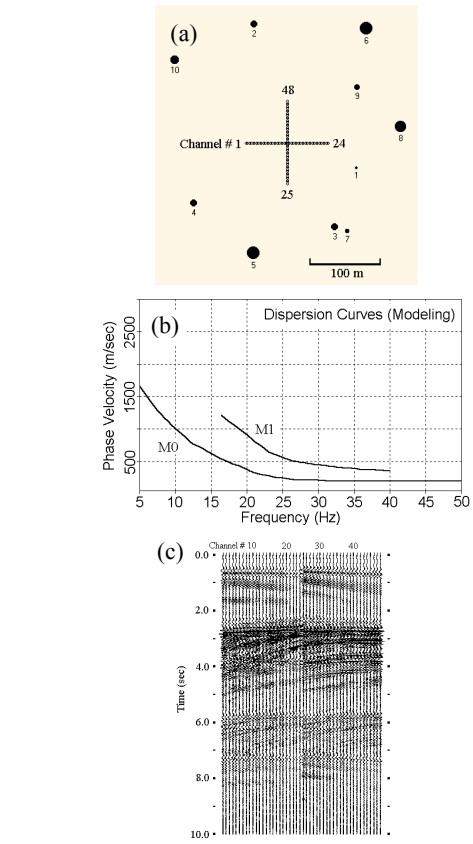

Figure 2. Location and strength (circle size) of sources (a) and dispersion curves (b) used to model a passive surface wave record (c).

Acknowledgments

We thank Mary Brohammer for her help in preparation of this manuscript.

References

Asten, M.W., and Henstridge, J.D., 1984, Array estimators and the use of microseisms for reconnaissance of sedimentary basins; Geophysics, 49, 1828-1837.

Haruhiko, H., and Hayashi, K., 2003, Shallow S-wave velocity sounding using the microtremors array measurements and the surface wave method; Proceedings of the SAGEEP 2003, San Antonio, TX, SUR08, Proceedings on CD ROM.

Louie, J.N., 2001, Faster, better: shear-wave velocity to 100 meters depth from refraction microtremor arrays; Bulletin of the Seismological Society of America, 2001, vol. 91, no. 2, p. 347-364.

Moro, G.D., Pipan, M., Forte, E., and Finnetti, I., 2003, Determination of Rayleigh wave dispersion curves for near surface applications in unconsolidated sediments; SEG Exp. Abs., 1247-1250.

Okada, H., 2003, The microtremor survey method; Geophysical monograph series, no. 12, published by Society of Exploration Geophysicists (SEG), Tulsa, OK.

Park, C.B., Miller, R.D., Xia, J., and Ivanov, J., 2004, Multichannel analysis of passive surface waves; in preparation for publication.

Park, C.B., Miller, R.D., and Xia, J., 1999, Multichannel analysis of surface waves (MASW); Geophysics, 64, 800-808.

Park, C. B., Xia, J., and Miller, R. D., 1998, Imaging dispersion curves of surface waves on multi-channel record; SEG Expanded Abstracts, 1377-1380.

Yoon, S., and Rix, G., 2004, Combined active-passive surface wave measurements for near-surface site characterization; Proceedings of the SAGEEP 2004, Colorado Springs, CO, SUR03, Proceedings on CD ROM.

Xia, J., Miller, R.D., and Park, C.B., 1999, Estimation of near-surface shear-wave velocity by inversion of Rayleigh waves: Geophysics, v. 64, no. 3, p. 691-700.

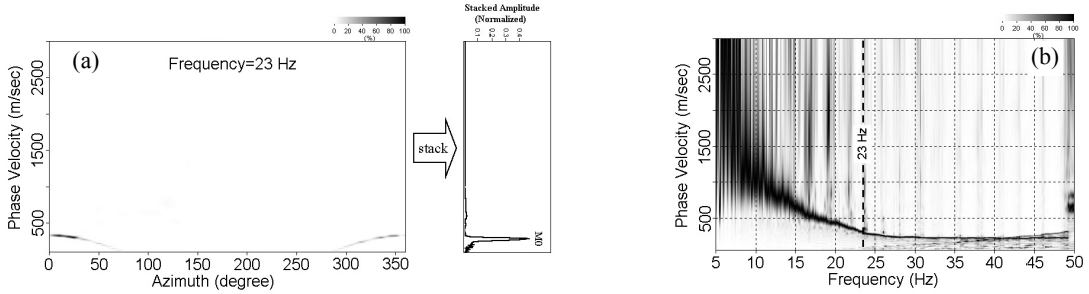

Figure 3. (a) Plane-wave energy (for 23 Hz) distribution of the modeled record in Figure 2c in phase velocity (*c*)-azimuth (θ) space. Energy stacked over all azimuths is displayed on right. (b) The dispersion image obtained from the model record in Figure 2c.

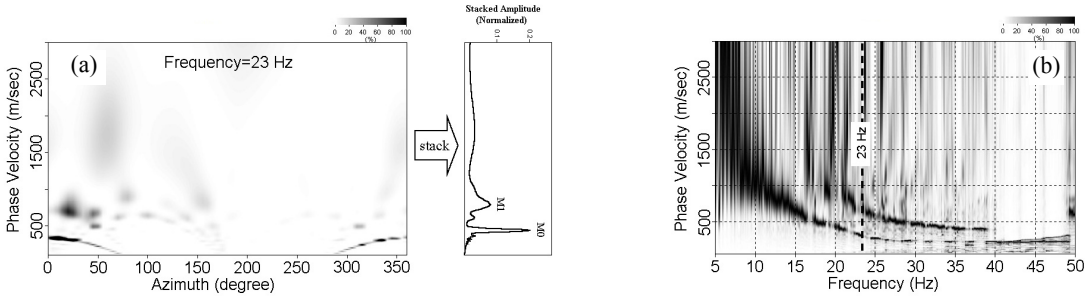

Figure 4. (a) Plane-wave energy (for 23 Hz) distribution of another modeled record (not shown) with two modes (M0 and M1) of dispersion. Energy stacked over all azimuths shows peaks at the correct phase velocities of the modeled modes. (b) The dispersion image obtained from the modeled record.

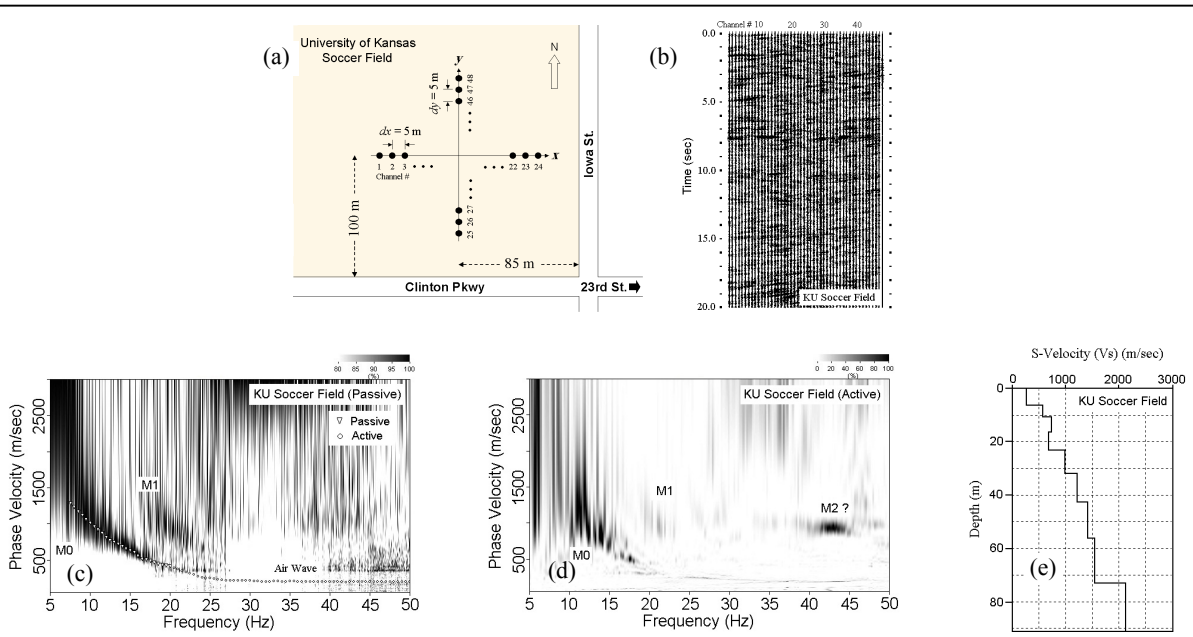

Figure 5. (a) Site map where passive surface wave data were acquired and a diagram of the cross-layout receiver spread. (b) A multi-channel record obtained by vertically stacking ten (10) individual field records of 20-sec recording time. (c) Dispersion images obtained from the field record in (b). (d) Dispersion images obtained from an active record. (e) S-wave velocity (Vs) profile from the inversion of the extracted dispersion curve marked in (c).